Evaluating the Accuracy of Jason-3 Water Vapor Product Using PWV Data from Global Radiosonde and GNSS Stations

Yangzhao Gong and Zhizhao Liu

Abstract—**Jason-3 is equipped with the Advanced Microwave Radiometer-2 (AMR-2) to account for the zenith wet delay (ZWD) caused by the troposphere in the altimeter signal, from which the precipitable water vapor (PWV) can be deduced. In order to investigate the accuracy of PWV from Jason-3 AMR-2 on a global scale, we adopt PWV observations from 263 radiosonde stations and 103 GNSS stations as reference PWV. These reference PWV are recorded during Jason-3 cycles 0 – 119 and are globally distributed in coastal and island regions. Over 60,000 Jason-3 PWV vs radiosonde PWV comparison points and over 380,000 Jason-3 PWV vs GNSS PWV comparison points are used in this study. For GNSS PWV, two PWV height reduction methods (Kouba empirical method and ECMWF method) are used to reduce PWV from height of station to sea level. The comparison results indicate that the root mean square error (RMSE) of Jason-3 PWV evaluated using radiosonde PWV is 3.4 kg/m^2. Jason-3 PWV has an RMSE of 3.0 kg/m^2 with GNSS PWV derived using ECMWF PWV height correction, while the RMSE between Jason-3 PWV and GNSS PWV derived using Kouba PWV height correction is 3.1 kg/m^2. In addition, the accuracy of Jason-3 PWV increases when the latitude of its footprints or the distance from its footprints to land increases.**

Index Terms—**Jason-3, Advanced Microwave Radiometer-2 (AMR-2), precipitable water vapor (PWV), global navigation satellite systems (GNSS), radiosonde.**

I. INTRODUCTION

AS an essential component of atmosphere, precipitable water vapor (PWV) plays an important role in climate change [1], protecting environment [2], radio-based geodetic technique [3], and many other areas. Currently, ground-based PWV observation systems, such as Global Navigation Satellite Systems (GNSS) networks, have provided a large volume of PWV data over continental lands, particularly in the northern hemisphere. However, it is challenging to make PWV observation over the vast ocean regions. In the oceanographic and geodetic community, a number of satellite missions have been launched, such as the altimetry satellites [4], [5]. These satellites normally are equipped with a microwave radiometer in order to correct the path delay caused by the water vapor and cloud liquid water content in the troposphere. This so-called zenith wet delay (ZWD) can be further converted to PWV using a conversion factor [6]. Normally, this conversion factor (the ratio of ZWD/PWV) has a value in the range of 6.0 to 7.0 depending on the local meteorological conditions [6], [7]. In addition to the correction of altimetry data, water vapor radiometers onboard altimetry satellites offer a valuable source of water vapor measurements over the vast ocean regions. These measurements, complementing the ground-based water vapor observations, make a significant contribution to the weather forecasting, climate studies and others.

Skylab, equipped with the first experimental altimeter, was launched in May 1973. However it was decommissioned very soon in 1974. The GEOSAT (GEOdetic SATellite) is the first altimetry mission that provided long-term altimetry observations. It was launched in March 1985 and ended its services in January 1990. After that, a series of altimetry missions were launched or are planned. These altimetry missions are summarized in TABLE I. Among the current altimetry missions, Jason-3 has relatively short repeat orbit (around 9.9 days). This means that Jason-3 can provide PWV observations with higher temporal resolution. Additionally, the Jason-3 is equipped with a 3-band radiometer, while the radiometers onboard Sentinel–3A, Sentinel-3B and SARAL (Satellite with ARgos and ALtiKa) work in 2-band [8]. Another altimetry mission with 3-band radiometer is the HY-2A [9]. No radiometer is embarked on Cryosat-2. In this study, Jason-3 is selected to be evaluated because of its superior performance in PWV monitoring.

Jason-3 satellite was launched by a joint mission by the Centre National d'Études Spatiales (CNES), the United States National Aeronautics and Space Administration (NASA), the European Organisation for the Exploitation of Meteorological Satellites (EUMETSAT) and the National Oceanic and Atmospheric Administration (NOAA) on 17 January 2016. It is the follow-on mission to the TOPEX/Poseidon, Jason-1, and OSTM/Jason-2 and is the 4th satellite in the TOPEX/Poseidon and Jason series. It takes an important responsibility of monitoring the change of sea level and collecting the oceanic

The authors are with the Department of Land Surveying and Geo-Informatics, The Hong Kong Polytechnic University, Kowloon, Hong Kong (e-mail: 18105647r@connect.polyu.hk, lszzliu@polyu.edu.hk). They are also affiliated with the also with the Research Institute for Sustainable Urban Development, The Hong Kong Polytechnic University, Hong Kong. Corresponding author: Zhizhao Liu.

meteorological observations. To monitor the change of sea level accurately, a 3-channel Advanced Microwave Radiometer-2 (AMR-2) operating at frequencies 18.7, 23.8, and 34.0 GHz is used at Jason-3 to correct the ZWD caused by water vapor along the signal path [5], [10], [11]. Compared with AMR onboard on OSTM/Jason-2, the Jason-3 AMR-2 is more stable and has better performance in instrument thermal control [5]. The Jason-3 AMR-2 is expected to have a better performance than its previous generation on TOPEX and Jason satellites, i.e., TOPEX/Poseidon Microwave Radiometer (TMR), Jason-1 Microwave Radiometer (JMR) as well as OSTM/Jason-2 AMR.

TABLE I
A LIST OF PAST, CURRENT, FUTURE ALTIMETRY MISSIONS

	Altimetry mission	Launch date – Decommission date
Past missions	Skylab	1973-1974
	GEOSAT (GEOdetic SATellite)	1985-1990
	ERS-1 (European Remote Sensing Satellite-1)	1991-1996
	TOPEX/Poseidon	1992-2005
	GFO (Geosat Follow-On)	1998-2008
	ERS-2	1995-2011
	Envisat (Environmental Satellite)	2002-2012
	Jason-1	2001-2013
	Ocean Surface Topography Mission (OSTM)/Jason-2	2008-2019
Current missions	Cryosat-2	2010-present
	HY-2A (Haiyang-2A)	2011-present
	SARAL (Satellite with ARgos and ALtika)	2013-present
	Jason-3	2016-present
	Sentinel-3A	2016-present
	Sentinel-3B	2018-present
Future missions	SWOT (Surface Water Ocean Topography)	Planned in 2021
	Jason-CS/Sentinel-6 (Including 2 satellites)	Jason-CS/Sentinel-6A: planned in 2020 Jason-CS/Sentinel-6B: planned in 2026
	Guanlan	Planned by China

However, we find that investigation on the performance of Jason-3 AMR-2 is very little. A study reported by Fernandes and Lázaro showed that Jason-3 ZWD has a root mean square error (RMSE) of 1.3 cm compared with Sentinel-3A ZWD [11]. For the previous missions, a large number of comprehensive evaluations have been conducted to analyze the accuracy of ZWD from TOPEX/Poseidon TMR, Jason-1 JMR and OSTM/Jason-2 AMR [12]–[15]. Ruf et al. [12] in 1994 estimated that the RMSE of TOPEX/Poseidon TMR measured ZWD was at around 1.1 cm by making comparison with ZWD from ground-based microwave water vapor radiometers and radiosonde. Keihm et al. [16] evaluated the performance of TOPEX/Poseidon TMR during 1992-1996 using the ZWD from 15 island radiosondes and the special sensor microwave imager (SSM/I) instruments. Based on the comparison results, they concluded that the scale error of TMR ZWD is no more than 2% [16]. For Jason-1 JMR, evaluations have also been conducted in the past studies. In 2003, an experiment at Harvest, California, USA (34.47° N, 120.67° W) showed that 1 cm-level agreement was found between both TMR ZWD and JMR ZWD and GNSS ZWD [17]. Compared with Jason-1 JMR, OSTM/Jason-2 AMR has been proved to have a more stable performance [18]. Sibthorpe et al. [15] compared ZWD from OSTM/Jason-2 AMR at 148 GNSS stations located at islands and coasts and a 6% of scale difference between OSTM/Jason-2 ZWD and GNSS ZWD was reported.

Previous studies have demonstrated that radiometers aboard on TOPEX/Jason series satellites are able to achieve a satisfying accuracy. However, the radiometer's performance degraded dramatically near the land because of significantly different emissivities for land (over 0.9) and for ocean (near 0.5) between 18 to 34 GHz [19]. Given the accuracy degradation caused by land contamination, ZWD measurements of Jason-2 near coastal regions are flagged as invalid if that contamination leads to ZWD difference larger than 5 mm when compared to the backup ZWD from ECMWF (the European Centre for Medium range Weather Forecasts) [15], [19]. Normally, the ZWD values of TOPEX/Poseidon TMR and Jason-1 JMR are treated as invalid when the distance between their footprints and coastlines is shorter than 50 km, while the corresponding distance is around 25 km for OSTM/Jason-2 AMR [19]. In order to improve the accuracy of OSTM/Jason-2 ZWD product near coastline, an improved ZWD retrieval algorithm was developed [19]. Using this algorithm, the ZWD error can be smaller than 0.8 cm, 1.0 cm, 1.2 cm when the footprint of OSTM/Jason-2 AMR is 15 km, 10 km, 5 km far from land, respectively. At the coastline, the error can be smaller than 1.5 cm using this algorithm [19]. Other attempts have also been made to improve the accuracy of altimetry satellite ZWD in the coastal regions by using ground-based GNSS observations [8], [20].

Recently, several studies utilized shipborne GNSS PWV to evaluate the accuracy of altimetry satellites, e.g. HY-2A, SARAL. Liu et al. [9] reported a 0.8 kg/m^2 difference between PWV derived from shipborne GPS/GLONASS observations and HY-2A calibration microwave radiometer (CMR) during a two-month cruise in the Indian Ocean. Wang et al. [21] used shipborne GNSS observations from a 20-day cruise in Fram Strait to investigate the accuracy of SARAL satellite PWV. Their result indicated a 1.7 kg/m^2 of RMSE between GNSS and SARAL PWV. One drawback in those studies is that both the area of evaluation region and the amount of statistical observations are limited due to the limitation of observing platform.

In this paper, the performance of Jason-3 AMR-2 on a global scale was evaluated. In our experiment, the PWV derived from Jason-3 AMR-2 are evaluated using the PWV from 103 globally distributed GNSS stations and 263 radiosonde stations that are distributed in islands or coastal areas. Compared with previous studies, we used many more and well distributed PWV observations from GNSS and radiosonde stations collected over

a period of three years. Detailed and comprehensive comparison about the performance of Jason-3 AMR-2 in island and coastal regions will be presented in following sections.

The rest of paper is organized as follows. First, the data used and PWV retrieving methods will be introduced in the Section II. Next, the method of PWV height correction will be introduced in Section III. Then, detailed discussion and analyses of five evaluation scenarios are shown in Section IV. Finally, conclusions are summarized in Section V.

II. DATA DESCRIPTION AND METHODS

A. Jason-3 PWV

Jason-3 has a repeat period of around 9.9 days with 254 passes per cycle between latitude 66.15° S – 66.15° N. There are three families of Geophysical Data Records (GDR), i.e., Operational GDR, Interim GDR, and final GDR. The major differences among three products are their latency and quality. The final GDR products have the highest quality as they are generated using precise orbits, but it has the longest product latency (~ 60 days). In this work, Jason-3 ZWD with a sampling rate of 1 s from final GDR products is adopted. The Jason-3 ZWD values are then converted to PWV using a PWV conversion factor (PWV_{factor}) for comparison purpose [6]:

$$PWV = ZWD \times PWV_{factor} \qquad (1)$$

The PWV_{factor} can be calculated based on local meteorological parameters, i.e., temperature, relative humidity and pressure [6], [22], [23]:

$$PWV_{factor} = \frac{10^5}{461.495\left(k_2 - k_1\frac{M_w}{M_d} + \frac{k_3}{T_m}\right)} \qquad (2)$$

where k_1 = 77.6890 K/hPa, k_2 = 71.2952 K/hPa, k_3 = 375463 K^2/hPa are refractivity constants. M_w = 0.018016 kg/mol and M_d = 0.028964 kg/mol are the molar mass of water vapor and dry air, respectively. T_m is the weighted temperature, which can be calculated by [24]:

$$T_m = \frac{\int_{h_s}^{\infty}\frac{e}{T}dh}{\int_{h_s}^{\infty}\frac{e}{T^2}dh} \qquad (3)$$

where T refers to temperature in unit of Kelvin, e represents water vapor partial pressure in unit of hPa. The calculation expression of e is shown as follows [25]:

$$e = 6.1121(1.0007 + 3.46 \times 10^{-6}P) \cdot RH \cdot$$
$$exp\left\{\frac{[18.729 - (T - 273.15)/227.3] \cdot (T - 273.15)}{T - 15.28}\right\} \qquad (4)$$

where P is the total air pressure in unit of hPa and RH refers to relative humidity (unitless).

In this study, for each pair of Jason-3 PWV vs radiosonde PWV comparison points, the PWV_{factor} is calculated using the above formulas with meteorological parameters from radiosonde observations. For each pair of Jason-3 PWV vs GNSS PWV comparison points, the PWV_{factor} is calculated using meteorological parameters from the ECMWF model.

ZWD derived from Jason-3 cycle 1 is shown in Fig. 1. Also, the numbers of ZWD observations of Jason-3 GDR products from cycle 0 to cycle 119 are shown in Fig. 2. We can observe that all the data are complete except a small amount of data missing in a few cycles. It should be noted that the invalid observations flagged by land, sea ice and rain contamination have been excluded in this study. The variation of numbers of

ZWD observations may be attributed to the variation of numbers of invalid observations. More detailed characteristics about Jason-3 can be found at [5], [10].
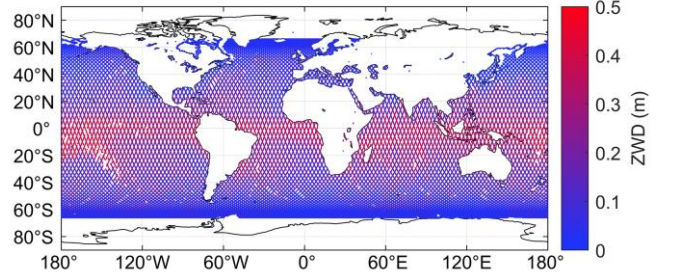

Fig. 1. ZWD of Jason-3 satellite during its cycle 1 from 17 February 2016 to 27 February 2016.
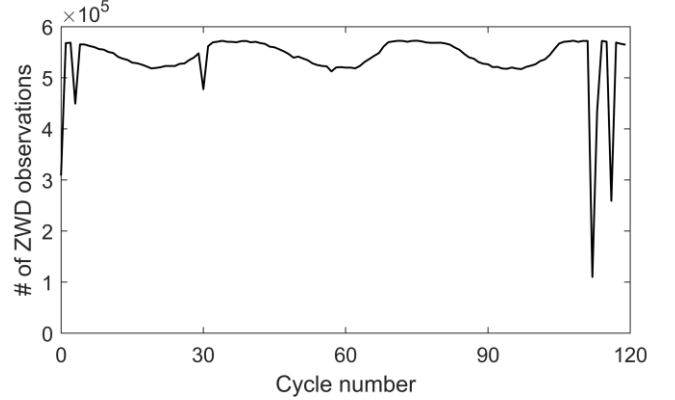

Fig. 2. Numbers of ZWD observation points of Jason-3 final GDR products during cycles 0-119. The observations flagged by land, sea ice, rain have been excluded.

B. Radiosonde PWV

Radiosonde is a traditional PWV observation system. It can measure meteorological parameters such as temperature, air pressure, and relative humidity at different altitudes over a radiosonde station. The PWV from radiosonde are normally treated as standard values to evaluate other PWV measurement techniques since it can achieve an accuracy of a few millimeters [26]. However, because of its high operation cost, the temporal resolution of radiosonde data is low. Meteorological balloons are normally released just twice a day at UTC 0 h and 12 h. A small number of stations also make radiosonde observations up to four times daily. Radiosonde data from 263 stations are used in this study. They are obtained from the Integrated Global Radiosonde Archive (IGRA). The IGRA provides meteorological profiles for over 2,700 stations worldwide including ~1,000 active stations that are still in operation.

Using meteorological profile, ZWD can be calculated as follows [27]:

$$ZWD = 10^{-6}\int_{h_s}^{\infty}N_w(h)\,dh \qquad (5)$$

where N_w is the atmospheric wet refractivity, which can be calculated by [27]:

$$N_w = \left(k_2 - k_1\frac{R_d}{R_w}\right)\frac{e}{T} + k_3\frac{e}{T^2} \qquad (6)$$

where k_1, k_2, k_3 have been defined in (2); e and T are derived from radiosonde profile, R_d = 287.053 J·K^{-1}·kg^{-1} and R_w = 461.495 J·K^{-1}·kg^{-1} are the gas constants of dry air and water vapor, respectively.

And then, radiosonde ZWD can be converted to PWV for comparison purpose. In this study, radiosonde PWV is selected

to compare Jason-3 PWV according to the criterion: temporal separation of radiosonde and Jason-3 PWV observations is no more than 30 minutes; their spatial separation is no more than 100 km. Following this criterion, a total of 263 radiosonde stations have been selected from the IGRA dataset. Their distribution is shown in Fig. 3.
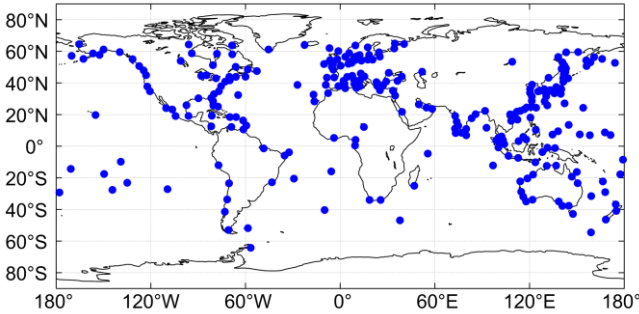

Fig. 3. Distribution of 263 radiosonde stations used for PWV comparison with Jason-3 observations.

C. ECMWF PWV

By assimilating various observations from a variety of earth observation systems such as GNSS stations, radiosonde stations, ocean buoys, ships, satellites, and aircrafts, ECMWF provides users with continuous, reliable, accurate meteorological grid products near the earth surface [28]. In this study, the ECMWF ERA-Interim reanalysis grid product in different pressure levels is used. This grid product provides meteorological parameters, i.e., temperature, relative humidity, pressure at each grid point at various pressure levels every 6 hours at UTC 0 h, 6 h, 12 h and 18 h since 1979 with a native spatial resolution of $0.75° \times 0.75°$. Users can interpolate or extrapolate the meteorological parameters to any location near the earth surface. The spatial resolution of ECMWF ERA-Interim reanalysis product used in this study is $1° \times 1°$.

D. GNSS PWV

GNSS is a powerful geodetic technique to monitor PWV. The International GNSS Service (IGS) provides high quality, final tropospheric product Zenith Troposphere Delay (ZTD) for over 400 stations worldwide on a daily basis [29]. The temporal resolution is as high as 5 minutes and its typical accuracy is 4 mm. In our study, the GNSS ZTD extracted from IGS products are interpolated to time point of Jason-3 PWV for comparison purpose. By a careful modeling and deduction of the zenith hydrostatic delay (ZHD) from GNSS ZTD, ZWD can be precisely obtained [30], [31]:

$$ZWD_{GNSS} = ZTD_{GNSS} - ZHD \qquad (7)$$

Subsequently PWV can be converted from ZWD using a PWV conversion factor.

The widely used empirical ZHD model, Saastamoinen model [32], is applied to remove the ZHD:

$$ZHD_{Saas} = \frac{0.0022768P_s}{(1 - 0.00266 \cos 2\varphi - 0.00028h_s)} \qquad (8)$$

where P_s refers to the air pressure at height of station in unit of hPa, which is obtained by interpolating or extrapolating ECMWF pressure profile in this study. φ is the station latitude in unit of radian and h_s is the height of station above sea level in unit of kilometer. Chen and Liu [33] reported that ZHD from the Saastamoinen model (ZHD_{Saas}) has an accuracy of 8.4 mm in China region.

Similar to the criterion of selecting radiosonde PWV data, only GNSS stations within 100 km of Jason-3 footprints are selected for PWV comparison. With such a criterion, 103 IGS stations globally distributed in coastal and island areas are selected, as shown in Fig. 4. As GNSS PWV has a high temporal resolution (5 min), GNSS PWV can be interpolated to every second of Jason-3 PWV observations.
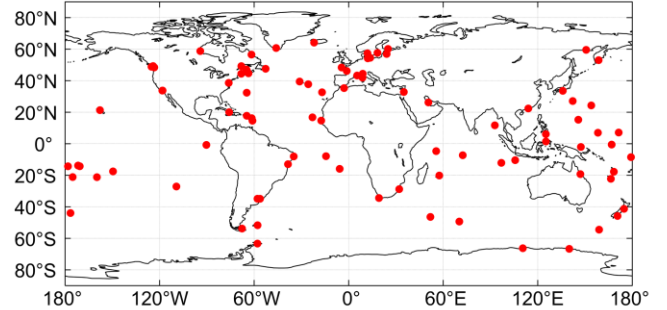

Fig. 4. Globally distributed 103 GNSS stations in island and coastal regions are selected from the IGS network for PWV comparison.

III. PWV HEIGHT CORRECTION

It should be noted that both radiosonde and GNSS PWV are referenced to their respective station heights while Jason-3 AMR-2 PWV are referenced to the sea level. In order to assess the Jason-3 PWV, all PWV observations should be reduced to the same altitude. In this work, the sea level is selected as the reference altitude and all the PWV are referenced to sea level. Our results show that the amount of PWV between the sea level and height of one GNSS station (22.24° N, 116.42° E, orthometric height 100 m) can be up to 2.2 kg/m^2 and apparently the PWV height correction for radiosonde and GNSS PWV data is not negligible. Detailed discussions regarding PWV height reduction have also been conducted in some previous studies [34], [35].

The reduction of the radiosonde PWV to sea level is relatively straightforward. By interpolating or extrapolating the meteorological parameters recorded by the radiosonde station itself, the PWV between station height and sea level can be calculated. It can then be used to reduce the radiosonde PWV to the sea level.

For GNSS PWV, the PWV reduction is relatively complex and two methods are studied in this study, as shown below. The first method, denoted as Kouba method, is to use the empirical equation [36]:

$$PWV_{hs} = PWV_{h0} \cdot exp\left(\frac{h_0 - h_s}{2000}\right) \qquad (9)$$

where PWV_{hs} and PWV_{h0} correspond to PWV at the elevation of station (h_s, unit: m) and sea level (h_0, 0 m in this study), respectively. This empirical equation can introduce 28% and 5% of reduction differences when the heights of station are 500 m and 100 m, respectively [8]. To minimize PWV contamination resulting from height correction, only those radiosonde and GNSS stations that have an orthometric height below 500 m are adopted in this study. The orthometric heights of radiosonde and GNSS stations are shown in Fig. 5, where it shows that most stations have a height below 100 m.

The second method, denoted as ECMWF method, is to interpolate or extrapolate the meteorological parameters from ECMWF ERA-Interim reanalysis products at an interval of 20

meters between the sea level and the height of GNSS station. Using formula (5), the ZWD between the station height and sea level can be calculated by an integration. This ZWD will be converted to PWV to reduce the GNSS PWV from their station height to sea level.
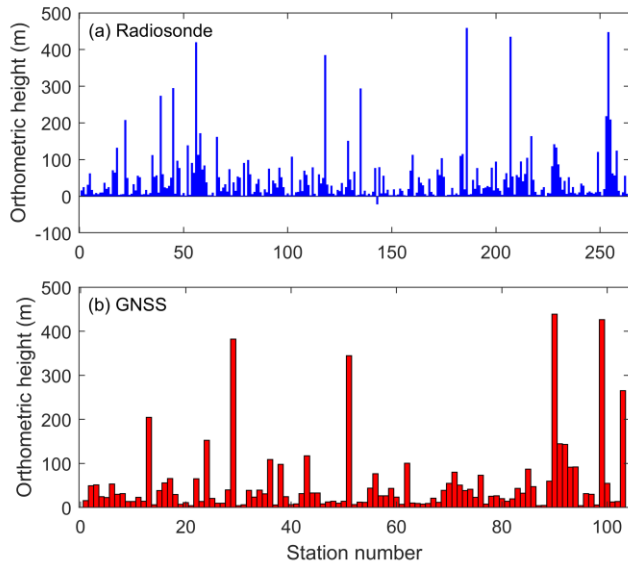

Fig. 5. The orthometric heights of radiosonde and GNSS stations

IV. RESULTS AND ANALYSES

A. Jason-3 average PWV at GNSS and radiosonde stations

The Jason-3 PWV values, observed with an interval of 1 s within 100-km vicinity of every radiosonde/GNSS station, are depicted in Fig. 6. Fig. 6(a) and (b) show that the PWV values in the low latitudes are much higher than those in the high latitudes. This is because of the high level of humidity in the equatorial region.
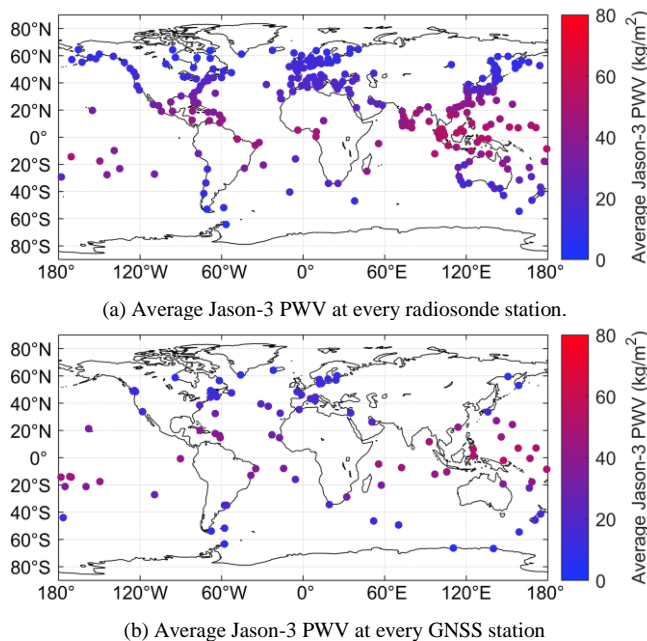

(a) Average Jason-3 PWV at every radiosonde station.

(b) Average Jason-3 PWV at every GNSS station

Fig. 6. Average Jason-3 PWV at radiosonde/GNSS stations during Jason-3 cycle 0 – cycle 119 (12 February 2016 - 12 May 2019).

B. Reducing radiosonde and GNSS PWV to sea level

Both radiosonde PWV and GNSS PWV are used to evaluate the accuracy of the Jason-3 PWV. The calculation of radiosonde PWV is straightforward and it is directly calculated from the meteorological parameters observed at each radiosonde station. To reduce the PWV from radiosonde height to sea level, meteorological parameters from radiosonde are interpolated or extrapolated first and they are then used to calculate the amount of PWV reduction.

For the calculation of GNSS PWV, two different schemes are studied to reduce the PWV from GNSS station height to sea level, as illustrated in TABLE II. They are: (1) in the first scheme, the ZHD is estimated using the Saastamoinen model and the Kouba method is used to reduce the PWV from GNSS station height to sea level; (2) the second scheme is very similar to the first scheme but the ECMWF method is used to reduce the PWV from GNSS station height to sea level.

TABLE II
THE SCHEMES OF REDUCING GNSS PWV FROM STATION HEIGHT TO SEA LEVEL

Scheme	Estimation of PWV	Method of reducing the PWV effect of GNSS station height to sea level
1	$(ZTD_{GNSS} - ZHD_{Saas}) \times PWV_{factor}$	Kouba method
2	$(ZTD_{GNSS} - ZHD_{Saas}) \times PWV_{factor}$	ECMWF method

C. Data quality control strategy

In order to obtain reliable comparison results, the quality of the PWV data should be controlled carefully. The algorithm error of deriving ZWD from Jason-3 AMR-2 data is <15 mm in coastal regions [10]. The uncertainty of final IGS ZTD products is around 4 mm [37]. In this study, we consider the accuracy of ZHD_{Saas} as 8.4 mm [33]. According to the error propagation law, the theoretical accuracy of ZWD differences between GNSS and Jason-3, i.e., $(ZTD_{GNSS}–ZHD_{Saas}–ZWD_{Jason-3})$, is about 18 mm (around 3.0 kg/m^2 in PWV). The accuracy of PWV difference between radiosonde and Jason-3 should be higher due to the higher accuracy of radiosonde PWV. Considering the spatial and temporal separation of two sets of PWV data as well as the error from station height PWV reduction, 10 kg/m^2 is defined as the threshold to detect outliers in PWV differences based on the 3σ rule. This means that those pairs of PWV comparisons larger than 10 kg/m^2 are regarded as outliers and excluded in this study.
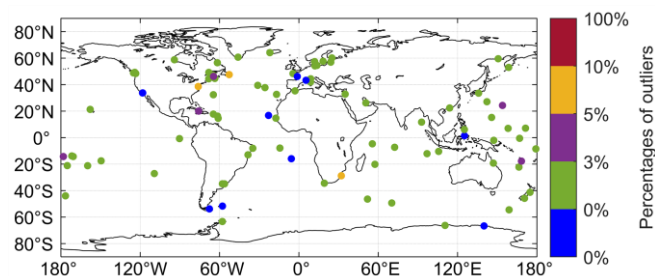
The numbers of total PWV observations and outliers are shown in TABLE III. It shows that only 2.7% of radiosonde PWV data are outliers. For the GNSS PWV data, the percentages of outliers are different depending on the scheme of PWV reduction method. The scheme 1 has the higher outlier percentage (1.0%) while the scheme 2 has 0.8% of outlier.

TABLE III
THE STATISTICS OF RADIOSONDE AND GNSS PWV DATA POINTS ACCORDING TO DIFFERENT LATITUDE REGIONS. THE PERCENTAGE DENOTES THE NUMBER OF
OUTLIERS OUT OF THE TOTAL NUMBER OF PWV OBSERVATIONS.

Latitude regions	Radiosonde		GNSS		
	# of PWV observations	# of PWV outliers	# of PWV observations Schemes 1 and 2	# of PWV outliers	
				Scheme 1	Scheme 2
20° S – 20° N	13655	603 (1.0%)	106634	1426 (0.4%)	1265 (0.3%)
20° N-40° N and 20° S – 40° S	18013	597 (1.0%)	77922	1105 (0.3%)	941 (0.2%)
40° N-70°N and 40° S-70° S	30748	428 (0.7%)	197008	1238 (0.3%)	1081 (0.3%)
Global	62416	1628 (2.7%)	381564	3769 (1.0%)	3287 (0.8%)

The percentage of the PWV data outliers at each radiosonde and GNSS station is shown in Fig. 7. Evidently, for most radiosonde/GNSS stations, the outlier percentage is no more than 3%. Stations with relatively high percentages of outliers are generally located in the low latitude region. This is probably because the humidity level in the low latitudes is high and the discrepancy between two types of PWV dataset more likely exceeds the 3σ criterion. The statistical results are also reported in TABLE IV. For radiosonde station, 123 radiosonde stations are free of outlier. Among the remaining 140 radiosonde stations, 48% of them (67) have outliers less than 3% and 29 stations have outliers more than 10%. For GNSS stations, 10 and 11 stations are free of outliers for scheme 1 and scheme 2, respectively. Over 80 GNSS stations have outliers no more than 3% in the two GNSS schemes.

(a) The percentage of PWV data outliers at every radiosonde station

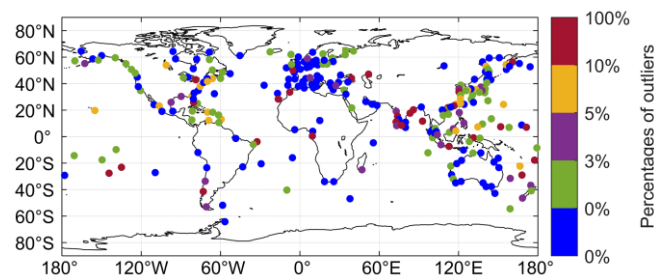(b) The percentage of PWV data outliers at every GNSS station in scheme 1

(c) The percentage of PWV data outliers at every GNSS station in scheme 2
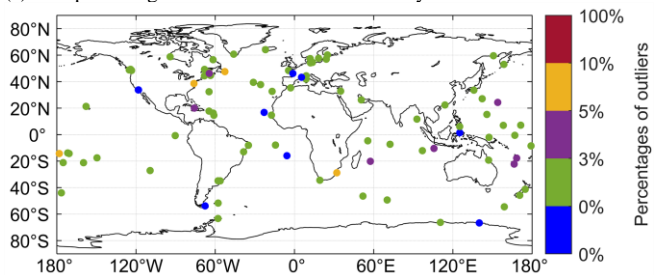Fig. 7. The percentages of PWV data outliers at every radiosonde/GNSS station.

TABLE IV
STATISTICS OF RADIOSONDE AND GNSS STATIONS IN EACH LEVEL OF
OUTLIER PERCENTAGE.

Percentages of outliers	Number of radiosonde stations	Number of GNSS stations	
		Scheme 1	Scheme 2
0%	123	10	11
(0% - 3%]	67	81	83
(3% -5%]	22	7	6
(5% - 10%]	22	5	3
(10% - 100%]	29	0	0
[0% - 100%]	263	103	103

D. Spatial assessment of Jason-3 PWV using radiosonde and GNSS PWV

The accuracy of Jason-3 PWV is evaluated using both radiosonde and GNSS PWV data. Both radiosonde and GNSS PWV have been reduced from their station heights to the sea level according to the approach in section IV-B. Fig. 8 shows the PWV RMSE of Jason-3 at 263 radiosonde stations and 103 GNSS stations over a period of more than 3 years from cycle 0 to cycle 119 (12 February 2016 to 12 May 2019). It is evident that most radiosonde and GNSS stations have a good agreement with Jason-3 PWV, although a few stations in the low latitude region have large RMSE. The percentages of radiosonde and GNSS stations for different PWV RMSE thresholds are shown in Fig. 9. We can observe that more than 70% of radiosonde stations have a PWV RMSE less than 4 kg/m^2. Around 90% of GNSS stations with schemes 1 and 2 have a PWV RMSE less than 4 kg/m^2.
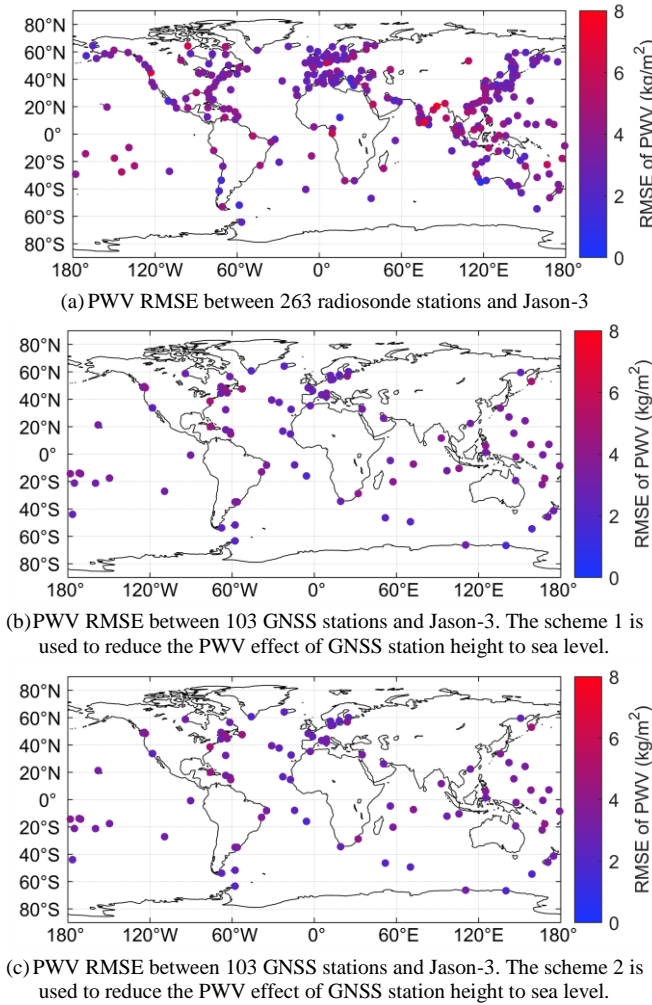
(a) PWV RMSE between 263 radiosonde stations and Jason-3

(b) PWV RMSE between 103 GNSS stations and Jason-3. The scheme 1 is used to reduce the PWV effect of GNSS station height to sea level.

(c) PWV RMSE between 103 GNSS stations and Jason-3. The scheme 2 is used to reduce the PWV effect of GNSS station height to sea level.

Fig. 8. RMSE between Jason-3 PWV and PWV from 263 radiosonde stations and 103 GNSS stations during Jason-3 cycles 0 –119 (12 February 2016–12 May 2019).
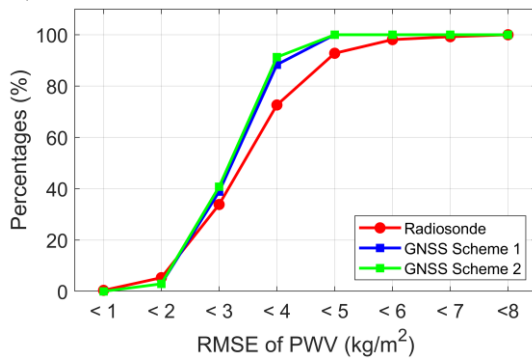

Fig. 9. The percentages of radiosonde and GNSS stations under different levels of PWV RMSE and different schemes.

E. RMSE of Jason-3 PWV data with respect to distance to land

In the Jason-3 GDR products, the radial distance from Jason-3 footprint to coastal land is also provided. The effect of such a radial distance on The PWV RMSE is studied on the basis of classification of their different values of radial distance: < 5 km, 5–10 km, 10–15 km, 15–25 km, 25–50 km, 50–100 km. As shown in Fig. 10, Jason-3 PWV evaluated using GNSS PWV with scheme 2 has the smaller RMSE compared to scheme 1, only the GNSS scheme 2 results are shown (Fig. 10 (b), (d), (f)).

It is noted that 3,177 radiosonde and 18,551 GNSS PWV comparison points are not included in the statistic because the radial distance exceeds 100 km for their radiosonde/GNSS stations.

We find that the RMSE of Jason-3 PWV generally decreases as the radial distance increases. Additionally, this is true in different latitude regions except the results evaluated by GNSS PWV in latitude $20°$–$40°$ S/N (Fig. 10 (d)). For instance, the Jason-3 PWV RMSE evaluated by the radiosonde at $40°$–$70°$ S/N decreases from 3.4 kg/m^2 to 2.7 kg/m^2 when the radial distance increases from <5 km to 50–100 km. Similarly, a decrease from approximately 3.0 kg/m^2 to 2.5 kg/m^2 is also observed with the results evaluated by GNSS PWV at $40°$–$70°$ S/N. One exception is shown in case of Fig. 10 (d). where the radial distance is < 5 km, the Jason-3 RMSE is actually smaller than the RMSE results that correspond to radial distance larger than 5 km. This is because the Jason-3 footprints are also very close to GNSS stations (approximately 35 km). The short separation between Jason-3 and GNSS stations explains the good agreement between Jason-3 and GNSS PWV in the < 5 km category.
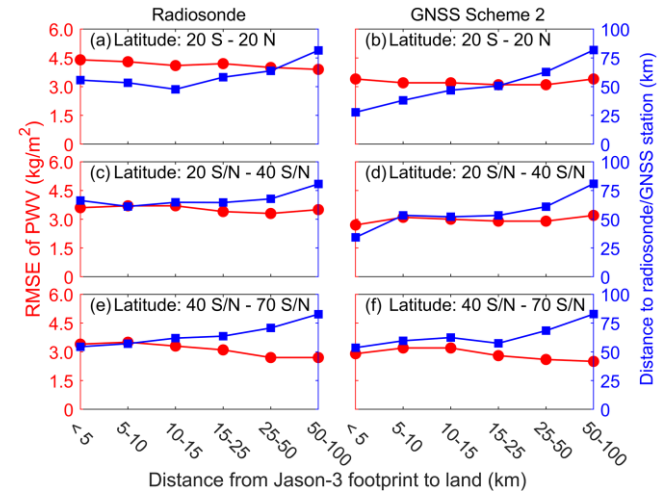

Fig. 10. The relationship between PWV RMSE and latitude and distance from Jason-3 footprints to land.

F. RMSE of Jason-3 PWV data with respect to latitude

We also find that the RMSE generally decreases with the increase of latitude, as shown in TABLE V. The Jason-3 PWV RMSE evaluated by radiosonde PWV are 4.0 kg/m^2, 3.5 kg/m^2, and 3.0 kg/m^2 at latitudes $20°$ S–$20°$ N, $20°$ S/N–$40°$ S/N, and $40°$ S/N–$70°$ S/N, respectively. Correspondingly the Jason-3 PWV RMSE evaluated by GNSS PWV (scheme 2) are 3.3 kg/m^2, 3.1 kg/m^2, and 2.8 kg/m^2 at latitudes $20°$ S–$20°$ N, $20°$ S/N–$40°$ S/N, and $40°$ S/N–$70°$ S/N, respectively.

The radiosonde in theory has the ability to measure PWV with an accuracy of 1-2 kg/m^2 [26]. The accuracy of Jason-3 PWV is ~2.5 kg/m^2 at coastlines, as discussed before. Thus the RMSE of Jason-3 PWV when evaluated by radiosonde is estimated to be ~3.0 kg/m^2. Considering the fact that the radiosonde station might not be exactly collocated with the Jason-3 footprints (spatial separation up to 100 km) and the radiosonde PWV might not be synchronously observed with Jason-3 PWV data (temporal separation up to 30 minutes), the

3.4 kg/m^2 RMSE of Jason-3 PWV using 263 global radiosonde stations is considered reasonable in this study.

As discussed in previous sections, the theoretical PWV RMSE of GNSS is ~3.0 kg/m^2. Considering that the GNSS station spatial separation from the Jason-3 footprints (up to 100 km) and that the error resulting from GNSS station height reduction to sea level, we think the RMSE of 3.1 kg/m^2 and 3.0 kg/m^2 shown in TABLE V for schemes 1 and 2, respectively, are reasonable.

TABLE V
RMSE (UNIT: KG/M^2), MEAN (THE FIRST NUMBER IN THE PARENTHESES, UNIT: KG/M^2) AND RELATIVE RMSE (THE PERCENTAGE IN THE PARENTHESES) OF PWV DIFFERENCE OF JASON-3 IN COMPARISON WITH RADIOSONDE AS WELL AS GNSS AT DIFFERENT LATITUDE REGIONS DURING THE JASON-3 CYCLES 0 – 119.

Latitude regions	Radiosonde	GNSS	
		Scheme 1	Scheme 2
20° S – 20° N	4.0 (3.3, 8.7%)	3.4 (2.7, 7.9%)	3.3 (2.6, 7.6%)
20° – 40° S and 20° – 40° N	3.5 (2.7, 12.6%)	3.1 (2.4, 11.6%)	3.1 (2.4, 11.3%)
40° – 70° S and 40° – 70° N	3.0 (2.3, 23.0%)	2.8 (2.2, 24.4%)	2.8 (2.2, 24.2%)
Global	3.4 (2.6, 13.8%)	3.1 (2.4, 13.0%)	3.0 (2.3, 12.7%)

G. Seasonal variation of RMSE of Jason-3 PWV data

Fig. 11 presents the monthly Jason-3 PWV RMSE evaluated with radiosonde and GNSS PWV during the entire 39-month period. It is evident that the PWV accuracy show a strong seasonal variation. All the monthly RMSE values become more significant in the summer months (north hemisphere) than winter months. This is particularly an event in the radiosonde evaluation results.

The monthly RMSE of Jason-3 PWV evaluated using radiosonde PWV exhibits the most significant monthly variation, varying from 2.5 kg/m^2 to 4.1 kg/m^2. Jason-3 PWV evaluated with GNSS schemes 1 and 2 has smaller monthly RMSE value. The monthly RMSE largely fluctuates around 3.0 kg/m^2.

As shown in Fig. 3, most of radiosonde stations are located in the northern hemisphere. In the summer months the magnitude of PWV is much larger than that in winter. Owing to the large variability of water vapor, the RMSE of PWV in the summer months is consequently larger. In comparison, the GNSS stations have a better distribution in both north and south hemisphere, as shown in Fig. 4. This explains that the summer and winter RMSE of Jason-3 evaluated using GNSS PWV demonstrate a less significant monthly variation.
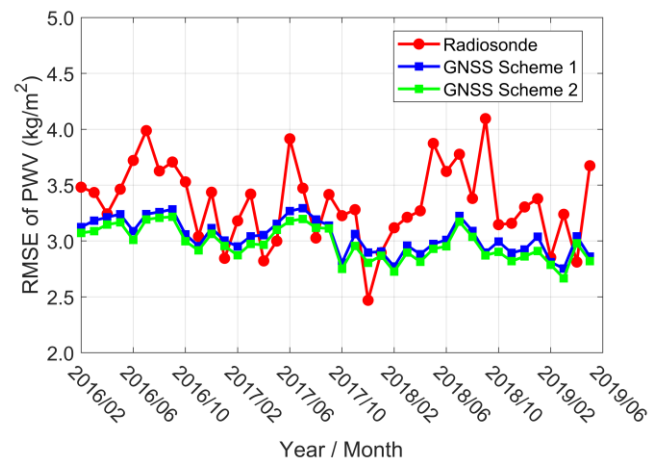

Fig. 11. Time series of monthly RMSE of Jason-3 PWV data in comparison with radiosonde and GNSS PWV during Jason-3 cycles 0–119 (12 February 2016–12 May 2019).

H. Scale error of Jason-3 PWV

To further investigate the agreement between Jason-3 PWV and radiosonde and GNSS PWV, the scatter plot of three PWV datasets are shown in Fig. 12. As shown in Fig. 12 (a), the linear fitting result indicates a slope of 0.98 between Jason-3 PWV and radiosonde PWV. This implies a 2% of scale difference between these two PWV datasets. Similarly, the linear fitting results between Jason-3 PWV and PWV from two GNSS schemes show a scale error of 3%.
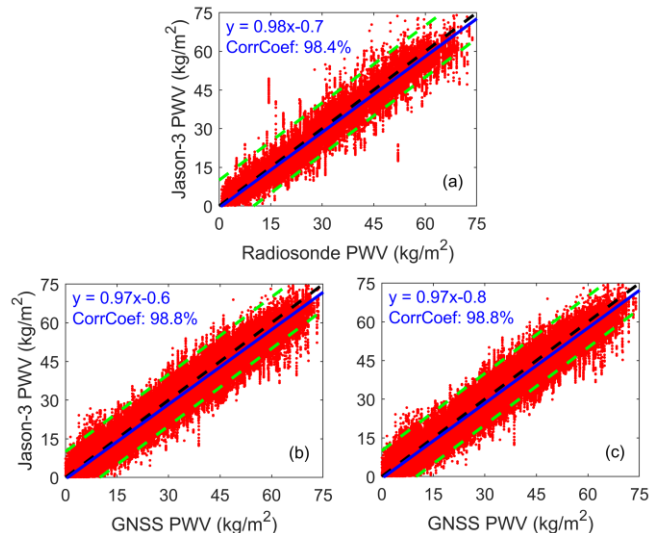

Fig. 12. Scatter plot of radiosonde and GNSS PWV against Jason-3 PWV during Jason-3 cycle 0 - cycle 119. Blue line is the linear fitting result. The black dashed line is y = x. The green dashed lines are the threshold lines (10 kg/m^2): y = x±10. (a) radiosonde, (b) GNSS PWV using station height PWV reduction scheme 1, (c) GNSS PWV using station height PWV reduction scheme 2.

V. CONCLUSION

Jason-3 is a relatively new altimetry satellite mission. A comprehensive assessment of its PWV at a global scale with multiple years of data is needed in order to fully understand its performance and capability. We used global PWV from 263 radiosonde stations and 103 GNSS stations, all of which are located in islands and coastal regions, to evaluate the Jason-3 PWV during its flight cycle 0 to cycle 119 (12 February 2016 - 12 May 2019). Over 60,000 radiosonde PWV comparison

points and over 380,000 GNSS PWV comparison points are used in this study. The percentages of outliers in radiosonde PWV and GNSS PWV data are 2.7% and 0.8%-1.0%, respectively. The outliers are discarded based on our data quality control criterion: PWV difference not exceeding 10 kg/m^2.

The accuracy of Jason-3 PWV is very consistent when evaluated by either radiosonde or GNSS. Globally the RMSE of Jason-3 PWV data is 3.4 kg/m^2 when compared to radiosonde PWV. The global RMSE are 3.0-3.1 kg/m^2 for two GNSS PWV processing schemes. Specifically, the GNSS scheme 2, i.e. use of ECMWF model to reduce the PWV from GNSS station height to sea level, is the better option (RMSE of 3.0 kg/m^2).

The RMSE of Jason-3 PWV increases when the Jason-3 footprints are closer to the land. This is mainly due to land contamination in the Jason-3 AMR-2 measurements. The RMSE increases as the latitude decreases. This is in agreement with the fact that the absolute values of PWV increase with the decrease of latitude. The RMSE of Jason-3 PWV shows evident seasonal variation, the RMSE in summer season (north hemisphere) larger than winter season.

REFERENCES

[1] L. Zhang, L. Wu, and B. Gan, "Modes and mechanisms of global water vapor variability over the twentieth century," *J. Clim.*, vol. 26, no. 15, pp. 5578–5593, Feb. 2013, doi: 10.1175/JCLI-D-12-00585.1.
[2] J. Wang, A. Dai, and C. Mears, "Global water vapor trend from 1988 to 2011 and its diurnal asymmetry based on GPS, radiosonde, and microwave satellite measurements," *J. Clim.*, vol. 29, no. 14, pp. 5205–5222, Apr. 2016, doi: 10.1175/JCLI-D-15-0485.1.
[3] J. Wang and Z. Liu, "Improving GNSS PPP accuracy through WVR PWV augmentation," *J. Geodesy*, Jul. 2019, doi: 10.1007/s00190-019-01278-2.
[4] J. Lambin *et al.*, "The OSTM/Jason-2 mission," *Mar. Geod.*, vol. 33, no. sup1, pp. 4–25, 2010, doi: 10.1080/01490419.2010.491030.
[5] F. Maiwald *et al.*, "Reliable and stable radiometers for Jason-3," *IEEE J. Sel. Top. Appl. Earth Observ. Remote Sens.*, vol. 9, no. 6, pp. 2754–2762, 2016.
[6] M. Bevis *et al.*, "GPS meteorology: Mapping zenith wet delays onto precipitable water," *J. Appl. Meteor.*, vol. 33, no. 3, pp. 379–386, 1994, doi: 10.1175/1520-0450(1994)033<0379:GMMZWD>2.0.CO;2.
[7] J. Stum, P. Sicard, L. Carrere, and J. Lambin, "Using objective analysis of scanning radiometer measurements to compute the water vapor path delay for altimetry," *IEEE Trans. Geosci. Remote Sens.*, vol. 49, no. 9, pp. 3211–3224, Sep. 2011, doi: 10.1109/TGRS.2011.2104967.
[8] J. Fernandes, C. Lázaro, M. Ablain, and N. Pires, "Improved wet path delays for all ESA and reference altimetric missions," *Remote Sens. Environ.*, vol. 169, pp. 50–74, Nov. 2015, doi: 10.1016/j.rse.2015.07.023.
[9] Y. Liu, Y. Liu, G. Chen, and Z. Wu, "Evaluation of HY-2A satellite-borne water vapor radiometer with shipborne GPS and GLONASS observations over the Indian Ocean," *GPS Solut.*, vol. 23, no. 3, p. 87, Jun. 2019, doi: 10.1007/s10291-019-0876-5.
[10] *Jason-3 products handbook*, 1.4 ed., SALP-MU-M-OP-16118-CN, 2017.
[11] M. J. Fernandes and C. Lázaro, "Independent assessment of sentinel-3A wet troposphere correction over the open and coastal ocean," *Remote Sens.*, vol. 10, no. 3, p. 484, 2018.
[12] C. S. Ruf, S. J. Keihm, B. Subramanya, and M. A. Janssen, "TOPEX/POSEIDON microwave radiometer performance and in-flight calibration," *J. Geophys. Res. Oceans*, vol. 99, no. C12, pp. 24915–24926, 1994, doi: 10.1029/94JC00717.
[13] S. Brown, C. Ruf, S. Keihm, and A. Kitiyakara, "Jason microwave radiometer performance and on-orbit calibration," *Mar. Geod.*, vol. 27, no. 1–2, pp. 199–220, 2004, doi: 10.1080/01490410490465643.
[14] D. P. Chambers, J. C. Ries, and T. J. Urban, "Calibration and verification of Jason-1 using global along-track residuals with TOPEX special issue: Jason-1 calibration/validation," *Mar. Geod.*, vol. 26, no. 3–4, pp. 305–317, Jul. 2003, doi: 10.1080/714044523.
[15] A. Sibthorpe, S. Brown, S. D. Desai, and B. J. Haines, "Calibration and validation of the Jason-2/OSTM advanced microwave radiometer using terrestrial GPS stations," *Mar. Geod.*, vol. 34, no. 3–4, pp. 420–430, 2011, doi: 10.1080/01490419.2011.584839.
[16] S. J. Keihm, V. Zlotnicki, and C. S. Ruf, "TOPEX microwave radiometer performance evaluation, 1992-1998," *IEEE Trans. Geosci. Remote Sens.*, vol. 38, no. 3, pp. 1379–1386, May 2000, doi: 10.1109/36.843032.
[17] B. J. Haines, D. Dong, G. H. Born, and S. K. Gill, "The Harvest experiment: Monitoring Jason-1 and TOPEX/POSEIDON from a California offshore platform special issue: Jason-1 calibration/validation," *Mar. Geod.*, vol. 26, no. 3–4, pp. 239–259, 2003, doi: 10.1080/714044520.
[18] M. Ablain, S. Philipps, N. Picot, and E. Bronner, "Jason-2 global statistical assessment and cross-calibration with Jason-1," *Mar. Geod.*, vol. 33, no. sup1, pp. 162–185, 2010, doi: 10.1080/01490419.2010.487805.
[19] S. Brown, "A novel near-land radiometer wet path-delay retrieval algorithm: Application to the Jason-2/OSTM advanced microwave radiometer," *IEEE Trans. Geosci. Remote Sens.*, vol. 48, no. 4, pp. 1986–1992, Apr. 2010, doi: 10.1109/TGRS.2009.2037220.
[20] M. J. Fernandes, C. Lazaro, A. L. Nunes, N. Pires, L. Bastos, and V. B. Mendes, "GNSS-Derived path delay: An approach to compute the wet tropospheric correction for coastal altimetry," *IEEE Geosci. Remote Sens. Lett.*, vol. 7, no. 3, pp. 596–600, Jul. 2010, doi: 10.1109/LGRS.2010.2042425.
[21] J. Wang *et al.*, "Retrieving precipitable water vapor from shipborne multi-GNSS observations," *Geophys Res Lett*, vol. 46, no. 9, pp. 5000–5008, 2019, doi: 10.1029/2019GL082136.
[22] Y. Yuan, K. Zhang, W. Rohm, S. Choy, R. Norman, and C.-S. Wang, "Real-time retrieval of precipitable water vapor from GPS precise point positioning," *J. Geophys. Res.*, vol. 119, no. 16, pp. 10044–10057, 2014, doi: 10.1002/2014JD021486.
[23] J. M. Rüeger, "Refractive index formulae for radio waves," in *Proc. FIG XXII Int. Congr.*, Washington, D.C. USA, 2002, pp. 1–13.
[24] J. L. Davis, T. A. Herring, I. I. Shapiro, A. E. E. Rogers, and G. Elgered, "Geodesy by radio interferometry: Effects of atmospheric modeling errors on estimates of baseline length," *Radio Sci.*, vol. 20, no. 6, pp. 1593–1607, 1985, doi: 10.1029/RS020i006p01593.
[25] A. L. Buck, "New Equations for computing vapor pressure and enhancement factor," *J. Appl. Meteor.*, vol. 20, no. 12, pp. 1527–1532, Dec. 1981, doi: 10.1175/1520-0450(1981)020<1527:NEFCVP>2.0.CO;2.
[26] A. E. Niell *et al.*, "Comparison of measurements of atmospheric wet delay by radiosonde, water vapor radiometer, GPS, and VLBI," *J. Atmos. Oceanic Technol.*, vol. 18, no. 6, pp. 830–850, 2001, doi: 10.1175/1520-0426(2001)018<0830:COMOAW>2.0.CO;2.

[27] J. Askne and H. Nordius, "Estimation of tropospheric delay for microwaves from surface weather data," *Radio Sci.*, vol. 22, no. 03, pp. 379–386, May 1987, doi: 10.1029/RS022i003p00379.

[28] D. P. Dee *et al.*, "The ERA-Interim reanalysis: Configuration and performance of the data assimilation system," *Q. J. R. Meteorol. Soc.*, vol. 137, no. 656, pp. 553–597, 2011, doi: 10.1002/qj.828.

[29] G. Beutler, M. Rothacher, S. Schaer, T. Springer, J. Kouba, and R. Neilan, "The International GPS Service (IGS): An interdisciplinary service in support of earth sciences," *Adv. Space Res.*, vol. 23, no. 4, pp. 631–653, 1999.

[30] B. Chen and Z. Liu, "Global water vapor variability and trend from the latest 36 year (1979 to 2014) data of ECMWF and NCEP reanalyses, radiosonde, GPS, and microwave satellite," *J. Geophys. Res.*, vol. 121, no. 19, p. 11,442-11,462, 2016, doi: 10.1002/2016JD024917.

[31] M. J. Fernandes, N. Pires, C. Lázaro, and A. L. Nunes, "Tropospheric delays from GNSS for application in coastal altimetry," *Adv. Space Res.*, vol. 51, no. 8, pp. 1352–1368, Apr. 2013, doi: 10.1016/j.asr.2012.04.025.

[32] J. Saastamoinen, "Atmospheric correction for the troposphere and stratosphere in radio ranging satellites," *Geophys. Monogr. Ser.*, vol. 15, pp. 247–251, 1972.

[33] B. Chen and Z. Liu, "A comprehensive evaluation and analysis of the performance of multiple tropospheric models in China region," *IEEE Trans. Geosci. Remote Sens.*, vol. 54, no. 2, pp. 663–678, Feb. 2016, doi: 10.1109/TGRS.2015.2456099.

[34] J. M. Fernandes, C. Lázaro, L. A. Nunes, and R. Scharroo, "Atmospheric corrections for altimetry studies over inland water," *Remote Sens.*, vol. 6, no. 6, 2014, doi: 10.3390/rs6064952.

[35] T. Vieira, M. J. Fernandes, and C. Lázaro, "Independent assessment of on-board microwave radiometer measurements in coastal zones using tropospheric delays from GNSS," *IEEE Trans. Geosci. Remote Sens.*, vol. 57, no. 3, pp. 1804–1816, Mar. 2019, doi: 10.1109/TGRS.2018.2869258.

[36] J. Kouba, "Implementation and testing of the gridded Vienna Mapping Function 1 (VMF1)," *J. Geodesy*, vol. 82, no. 4, pp. 193–205, Apr. 2008, doi: 10.1007/s00190-007-0170-0.

[37] W. Li, Y. Yuan, J. Ou, H. Li, and Z. Li, "A new global zenith tropospheric delay model IGGtrop for GNSS applications," *Chin. Sci. Bull.*, vol. 57, no. 17, pp. 2132–2139, Jun. 2012, doi: 10.1007/s11434-012-5010-9.

Yangzhao Gong received the B.Sc. degree in surveying engineering from Xi'an university of Science and Technology, Xi'an, China, in 2015, the M.Sc. degree in geodesy from Central South University, Hunan, China, in 2018, He is currently an Ph.D. student in the Department of Land Surveying and Geo-Informatics, The Hong Kong Polytechnic University, Kowloon, Hong Kong.

His current research interests include GPS/GNSS atmosphere monitoring, GPS/GLONASS precise point positioning (PPP)

Zhizhao Liu received the B.Sc. degree in surveying engineering from Jiangxi University of Science and Technology, Ganzhou, China, in 1994, the M.Sc. degree in geodesy from Wuhan University, Wuhan, China, in 1997, and the Ph.D. degree in geomatics engineering from the University of Calgary, Calgary, Alberta, Canada, in 2004.

He is currently an Associate Professor with the Department of Land Surveying and Geo-Informatics, The Hong Kong Polytechnic University, Kowloon, Hong Kong. He is a guest Professor with Liaoning Technical University, Huludao, China, and Wuhan University. His research interests include new algorithm development for precise Global Positioning System (GPS) and Global Navigation Satellite System (GNSS), GPS/GNSS precise point positioning (PPP), ionosphere modeling and scintillation monitoring, tropospheric remote sensing and modeling, and GPS/GNSS meteorology. He has over 20 years of experience in GPS/GNSS research. His group developed China's first GPS PPP-based Precipitable Water Vapor Real-time Monitoring System in the Pearl-River-Delta region in 2012. His research group established Hong Kong's first GPS/GNSS-radiosonde water vapor sounding collocation system in 2013 in collaboration with Hong Kong Observatory. In 2012, his group developed Hong Kong's first GPS/GNSS-based ionosphere scintillation monitoring system (two stations deployed in South and North Hong Kong) with his collaborators.

Dr. Liu was the recipient of the inaugural Early Career Award of the Hong Kong Research Grants Council (RGC), Hong Kong, in 2012 and was the recipient of the inaugural Best Conference Paper of the China Satellite Navigation Conference (CSNC), China, in 2013. In 2014, he was nominated by the Hong Kong Observatory for the World Meteorological Organization (WMO) "Norbert Gerbier-MUMM International Award for 2015" for his paper that has developed a method to evaluate the absolute accuracy of water vapor measurements.